Tuning the magnetic properties of $La_{0.67}Sr_{0.33}CoO_{3-\delta}$ films by oxygen pressure

Bin Liu,[1] Yiqian Wang,[1,*] Guiju Liu,[1] Honglei Feng,[1] Huaiwen Yang,[2] Xuyan Xue,[1] and Jirong Sun[2]

[1]*College of Physics and The Cultivation Base for State Key Laboratory, Qingdao University, No. 308, Ningxia Road, Qingdao 266071, People's Republic of China*

[2]*Beijing National Laboratory for Condensed Matter Physics, Institute of Physics, Chinese Academy of Sciences, Beijing 100080, People's Republic of China*

In this paper, oxygen-deficient $La_{0.67}Sr_{0.33}CoO_3$ (LSCO) thin films are prepared by adjusting the oxygen pressure during the deposition. As oxygen vacancies are introduced into the LSCO films, the out-of-plane lattices are elongated, as revealed by x-ray diffraction and high-resolution transmission electron microscopy (HRTEM). Modulated bright and dark stripes observed in the HRTEM images of the oxygen-deficient LSCO films are induced by cation ordering and oxygen vacancy ordering, respectively. Magnetic measurements and first-principles calculations show that the oxygen vacancies depress the magnetism of the LSCO films greatly. We also demonstrate that doping Sr into $LaCoO_3$ and removing oxygen from LSCO have a similar effect on the magnetic properties, which is correlated with a derived formula.

I. INTRODUCTION

Transition metal oxides have attracted much attention for the unconventional phenomena they exhibit due to the strong interplay between spin, charge, orbital, and lattice degrees of freedom. The spin-state transitions in $LaCoO_3$-based perovskite oxides have been widely studied [1–6]. It has been demonstrated that the magnetism of perovskite cobalt oxides is sensitive to external and internal factors such as lattice strain, element doping, and oxygen nonstoichiometry. For example, the magnetic properties are very different when the $LaCoO_3$ films suffer from tensile or compressive strains [7–10], and the magnetization increases significantly with increasing tensile strain that favors high-spin-state Co^{3+} ions [11,12]. An unexpected dependence of the magnetization on Sr content was also observed in $La_{1-x}Sr_xCoO_3$ films [13]. The magnetization is weakened by introducing Sr ions into tensile $La_{1-x}Sr_xCoO_3$ film ($0.05 < x < 0.2$), rather than enhanced as it is for its bulk counterpart. In this case, Sr doping drives a high- to low-spin-state transition for the Co^{3+} ions, disfavoring ferromagnetic ordering [14].

Compared with the lattice strain and Sr doping, the effect of oxygen nonstoichiometry is of special interest. It is known that either doping Sr into $LaCoO_3$ or removing oxygen from LSCO can affect the Co^{3+}/Co^{4+} ratio in perovskite cobalt oxides. Although there are reports on the effect of oxygen nonstoichiometry on the magnetic properties of $La_{0.67}Sr_{0.33}CoO_{3-\delta}$ ($LSCO_{3-\delta}$) films [15], no special efforts have been devoted to investigate the connection between Sr doping and the introduction of an oxygen vacancy. Two methods can be used to produce oxygen vacancies in $La_{0.67}Sr_{0.33}CoO_3$ (LSCO) films: The first is annealing the film in vacuum after the ablation process [16], and the second is adjusting the oxygen pressure during the deposition [17]. In this paper, different oxygen-deficient LSCO films were prepared by the second method, and the effects of oxygen vacancies on the magnetic properties were studied. Combining first-principles calcula-

tions and transmission electron microscope (TEM) and magnetic measurements, we perform a systematic investigation on $LSCO_{3-\delta}$ films, focusing on the combined effects of Sr doping and oxygen nonstoichiometry on magnetism.

II. EXPERIMENTAL DETAILS

Different oxygen-deficient LSCO films were epitaxially grown on (001) $SrTiO_3$ (STO) and (001) $LaAlO_3$ (LAO) substrates using the pulsed laser deposition (PLD) technique from ceramic targets prepared by the solid state reaction. During the deposition, the substrate was maintained at 800 °C and the oxygen pressures at 0.01, 1, and 50 Pa, respectively, to tune the oxygen content in the resultant films. The laser wavelength was 248 nm, the pulse fluence was $1.5\,J/cm^2$, and the ablation frequency was 1 Hz. The film thickness is 50 nm, determined by the deposition time. After deposition, all films except for that obtained under 50 Pa were furnace cooled to room temperature under the deposition pressure. Before cooling to room temperature, the film prepared under 50 Pa was further heated at 800 °C for 2 h in an oxygen atmosphere of 10 bars to improve its oxygen stoichiometry.

Specimens for TEM examinations were prepared in cross-sectional orientations ([010] zone axis of the STO substrate) using conventional techniques of mechanical polishing and ion thinning. The ion milling was performed using a Gatan Model 691 precision ion polishing system (PIPS). The bright-field (BF) imaging, selected-area electron diffraction (SAED), and high-resolution TEM (HRTEM) examinations were carried out on a JEOL JEM2100F electron microscope operated at 200 kV. The chemical compositions of LSCO films prepared at different oxygen pressures were determined using energy-dispersive x-ray spectroscopy (EDS) in a JEOL JEM2100F TEM, which shows that the oxygen is stoichiometric only in the film prepared at 50 Pa. The film structure was analyzed by x-ray diffraction (Bruker x-ray diffractometer, $\lambda = 1.5406\,\text{Å}$). Owing to its high intensity, we chose the (002) reflection for a systematic analysis. The magnetic properties were measured using a commercial superconducting quantum interference device, vibrating-sample magnetometer (Quantum Design
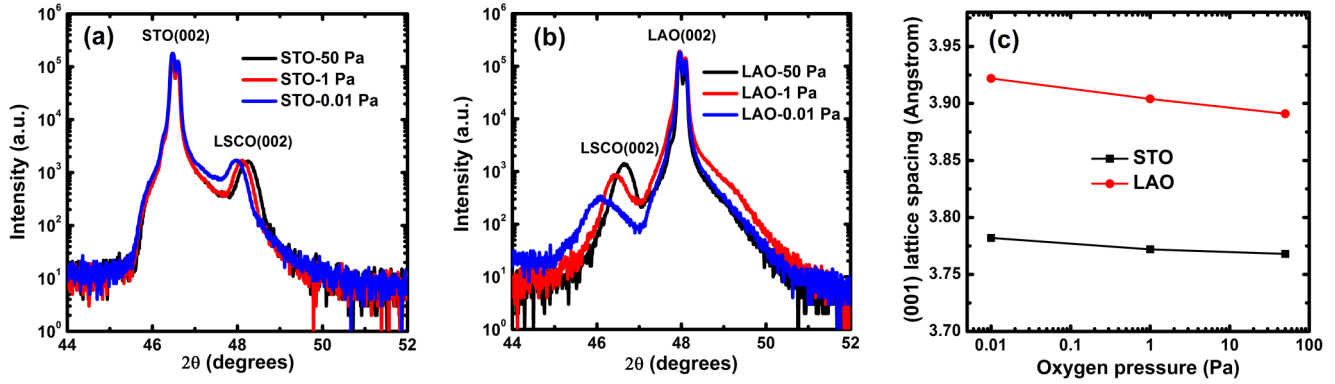
---

*Corresponding author: yqwang@qdu.edu.cn

FIG. 1. XRD patterns of 50-nm-thick LSCO films grown at different oxygen pressures on (a) STO and (b) LAO; (c) the out-of-plane lattice elongation of the films with changing oxygen pressures.

VSM-SQUID), in the temperature range 5–300 K under applied magnetic fields up to 7 T.

III. RESULTS AND DISCUSSION

To study the effect of oxygen content on both crystal structure and microstructure of the films, we carried out systematic investigations using XRD and TEM. Figures 1(a) and 1(b) show the XRD patterns of the LSCO films grown under different oxygen pressures on the STO or LAO substrate. Consistent with previous reports [18,19], the (002) reflections of the films on both substrates shift to small angles with decreasing oxygen pressure, indicating an out-of-plane lattice expansion as shown in Fig. 1(c). Decreasing oxygen pressure from 50 Pa to 1 Pa and 0.01 Pa, for example, the (001) lattice constant increases from 3.768 Å to 3.772 Å and 3.782 Å for the LSCO/STO films. Since the (001) lattice elongation is less than 0.032 Å, the content of oxygen vacancies (δ) in the $LSCO_{3-\delta}$ film can be estimated by [20]

$$\delta = \frac{6.41 \Delta d}{\sqrt{2}}, \qquad (1)$$

where Δd is the out-of-plane lattice expansion caused by the oxygen deficiency. $\sqrt{2}$ is introduced because the definition of the lattice constant here is different from that in Ref. [20]. For the $LSCO_{3-\delta}$/STO films prepared at 1 and 0.01 Pa, δ is calculated to be 0.018 and 0.063, respectively, according to Eq. (1), thus the ionic states of two films are determined to be $La_{0.67}^{3+}Sr_{0.33}^{2+}Co_{0.71}^{3+}Co_{0.29}^{4+}O_{2.98}^{2-}$ and $La_{0.67}^{3+}Sr_{0.33}^{2+}Co_{0.79}^{3+}Co_{0.21}^{4+}O_{2.94}^{2-}$, respectively. In the same way, the ionic structures of $LSCO_{3-\delta}$/LAO films grown at 1 and 0.01 Pa are calculated to be $La_{0.67}^{3+}Sr_{0.33}^{2+}Co_{0.79}^{3+}Co_{0.21}^{4+}O_{2.94}^{2-}$ and $La_{0.67}^{3+}Sr_{0.33}^{2+}Co_{0.96}^{3+}Co_{0.04}^{4+}O_{2.86}^{2-}$, respectively. To verify the out-of-plane lattice elongation obtained from XRD, the (001) lattice distances were further investigated by HRTEM. Figures 2(a) and 3(a) show the cross-sectional BF TEM images of the LSCO/STO films grown at 50 and 0.01 Pa, respectively. White arrows indicate the interface between the film and the substrate. As clearly observed, both films are ∼50 nm thick and their surfaces are smooth. However, a second phase (labeled with black arrows) is formed in the film grown at 0.01 Pa. The SAED patterns of the LSCO/STO films grown at 50 and 0.01 Pa are shown in Figs. 2(b) and 3(b), respectively, which

can be indexed using a pseudocubic unit cell ($a = 3.82$ Å). Some dots which should be extinct (marked by white arrows)
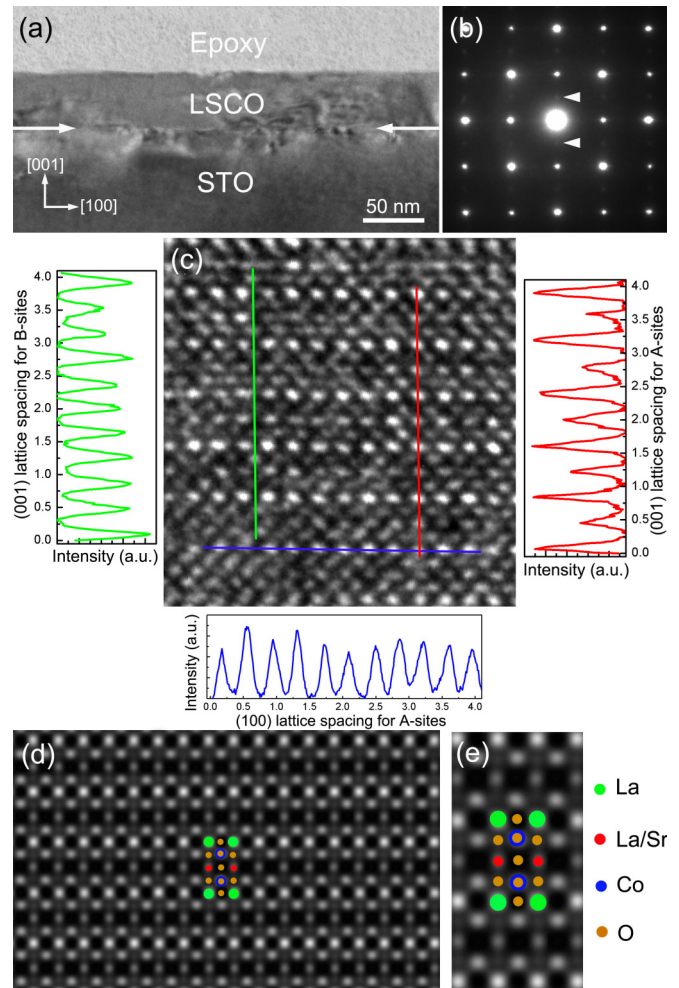

FIG. 2. (a) Cross-sectional BF image, (b) SAED pattern, and (c) typical HRTEM image of the LSCO/STO film grown at 50 Pa. The red and blue lines represent the La-O planes and the green line represents the Co-O planes. Three insets show the intensity profiles for the corresponding lines. (d) Simulated image of LSCO film with $\Delta f = -54.0$ nm and $t = 24.6$ nm, and (e) the enlarged simulation image.
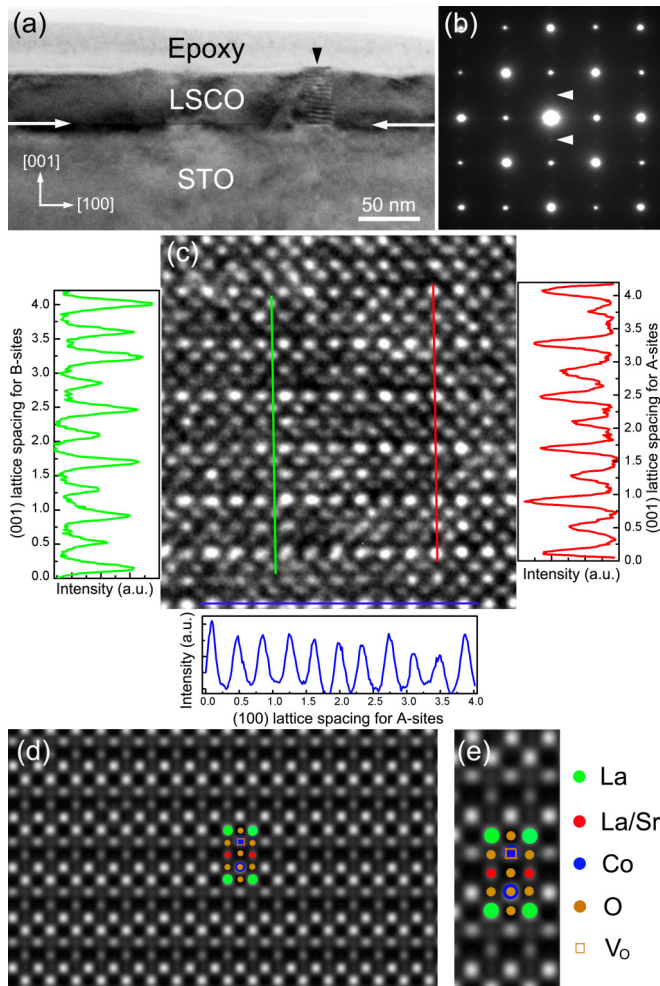
FIG. 3. (a) Cross-sectional BF image, (b) SAED pattern, and (c) typical HRTEM image of the LSCO$_{3-\delta}$/STO film grown at 0.01 Pa. The red and blue lines represent the La-O planes and the green line represents the Co-O planes. Three insets show the intensity profiles for the corresponding lines. (d) Simulated image of LSCO$_{3-\delta}$ film with $\Delta f = -69.0$ nm and $t = 34.9$ nm, and (e) the enlarged simulation image.

appear at half-positions between the fundamental reflections in both patterns. The wave vector of these dots is $[\frac{1}{2},0,0]$, which represents a modulated structure with a periodicity twice the original lattice parameter. Figures 2(c) and 3(c) show typical HRTEM images of the LSCO/STO films grown at 50 and 0.01 Pa, respectively. For the film grown at 50 Pa, the (001) and (100) lattice spacings are measured to be 3.76 and 3.77 Å, respectively, from the insets of Fig. 2(c), while for the film grown at 0.01 Pa, the (001) and (100) lattice spacings are measured to be 3.79 and 3.74 Å, respectively, from the insets of Fig. 3(c). Thus the (001) lattice spacing of the films is elongated from 3.76 to 3.79 Å when the oxygen pressure decreases from 50 to 0.01 Pa, which is consistent with the XRD results. Meanwhile, in the LSCO film prepared at 50 Pa, only one type of modulated stripe in A sites (La-O planes in LSCO, labeled by the red line) is observed in Fig. 2(c). Systematic HRTEM simulations were performed and one simulated image with $\Delta f = -54.0$ nm (defocus value) and $t = 24.6$ nm (thickness) is shown in Fig. 2(d). In B sites, no contrast difference can be found between pure Co^{3+} planes and Co^{4+}/Co^{3+} mixed planes. On the other hand, in A sites, the pure La^{3+} planes have stronger intensity than the La^{3+}/Sr^{2+} mixed planes. Therefore, the appearance of modulated stripes in the stoichiometric LSCO film is derived from the cation ordering of La^{3+} and Sr^{2+}, while in the LSCO film prepared at 0.01 Pa, in addition to the stripes in A sites, weak stripes in B sites (Co-O planes in LSCO$_{3-\delta}$, labeled by the green line) are clearly shown in Fig. 3(c), which is consistent with the work of Donner *et al.* [21]. Donner *et al.* found that the intensity of the half-order reflection results not only from an ordering of the oxygen vacancy planes, which could only lead to weak superstructure reflections, but also from the A-site ordering; this was confirmed by structure factor calculations. The simulated HRTEM image [Fig. 3(d)] agrees well with the experimental one. In A sites, the intensity of pure La^{3+} planes is stronger than that of La^{3+}/Sr^{2+} mixed planes; in B sites, the Co-O planes containing oxygen vacancies are weaker than the others. Therefore, we believe that weak stripes in B sites are induced by the oxygen vacancy ordering.

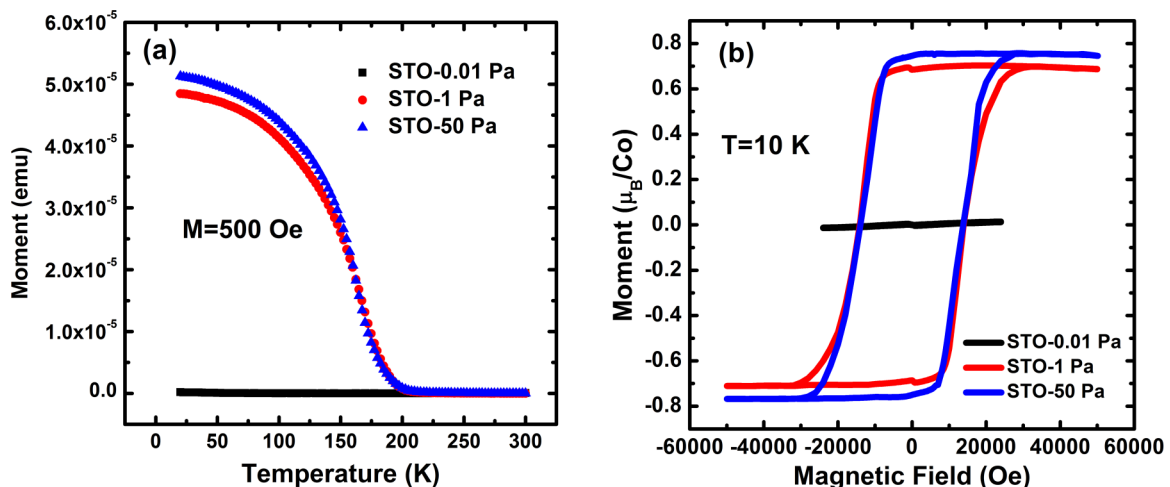Figure 4(a) shows the temperature-dependent magnetization (M-T) curve measured under an applied field of 500 Oe

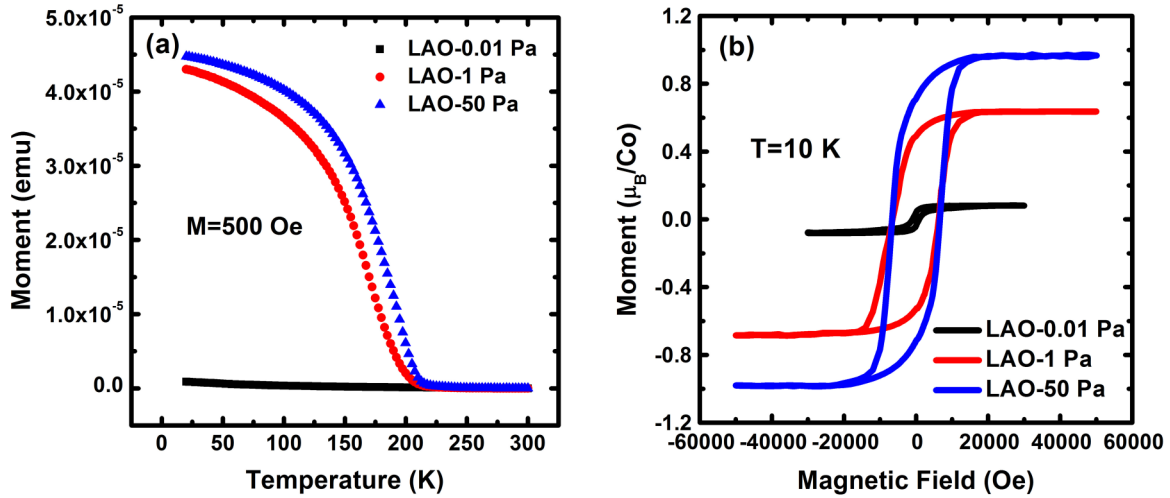FIG. 4. (a) M-T and (b) M-H curves for LSCO/STO films grown at different oxygen pressures.

FIG. 5. (a) *M-T* and (b) *M-H* curves for LSCO/LAO films grown at different oxygen pressures.

in the temperature range 20–300 K. A typical paramagnetic-ferromagnetic transition appears at ~175 K for the LSCO/STO films grown under oxygen pressures of 1 and 50 Pa. In contrast, no magnetic order is observed in the film grown under 0.01 Pa pressure. The saturation magnetization can be deduced from the magnetic loops (*M-H*) measured at 10 K [Fig. 4(b)]; it varies from $0.76\,\mu_B$/Co to $0.7\,\mu_B$/Co when oxygen pressure decreases from 50 to 1 Pa. For the film grown under 0.01 Pa pressure, the magnetization is very small and varies linearly with applied field. These results indicate that the ferromagnetism of the LSCO/STO films is suppressed by introducing oxygen vacancies into the film. For comparison, the *M-T* and *M-H* curves were also measured for the LSCO/LAO films grown at different oxygen pressures, as shown in Fig. 5. The magnetic moment of the films saturates at $0.98\,\mu_B$/Co at 50 Pa and drops drastically when the oxygen pressure decreases to 0.01 Pa, which is similar to the behavior observed in LSCO$_{3-\delta}$/STO films.

To confirm the effect of oxygen vacancies on the magnetization, first-principles calculations were performed [22], combined with projector augmented wave (PAW) method [23] in the Vienna *ab initio* simulation package (VASP) code. In the oxygen stoichiometric LSCO, 12 Co cations can be considered as six low spin (LS) Co^{3+} ($t_{2g}^6 e_g^0$, $S = 0$), two intermediate spin (IS) Co^{3+} ($t_{2g}^5 e_g^1$, $S = 1$), and four LS Co^{4+} ($t_{2g}^5 e_g^0$, $S = \frac{1}{2}$), as shown in Fig. 6(a). Using these parameters, the calculated total magnetization is $9.72\,\mu_B$ and the average magnetization is $0.81\,\mu_B$/Co, which is consistent with the experimental results. While introducing one oxygen vacancy into the unit cell [as shown in Fig. 6(b)], the total magnetic moment decreases drastically to $3.4\,\mu_B$. Only two Co atoms remain to possess a magnetic moment of $1.7\,\mu_B$, which can be regarded as IS Co^{3+}, whereas the others have a magnetic moment of nearly $0\,\mu_B$. The introduction of an oxygen vacancy has two effects: The LS Co^{4+} turns into LS Co^{3+}, and a CoO$_6$ octahedron is transformed into a CoO$_3$ tetrahedron. From the calculated density of states (DOS) for Co atoms in the oxygen-stoichiometric and oxygen-deficient LSCO films, as shown in Fig. 6(c), one can see that the spin polarization is different for these two films, and the oxygen-stoichiometric LSCO film has larger spin polarization. In other words,

the introduced oxygen vacancy strongly depresses the spin polarization of Co ions.

The Co^{4+}/Co^{3+} ratios in cobalt oxides can be controlled either by doping Sr into LaCoO$_3$ or by removing oxygen from LSCO. However, as reported in the literature [20], these two methods may not be equivalent. To find their underlying connections, we compare the present results with the relevant data available in the literature, which is summarized in Table I. We find that the LSCO$_{3-\delta}$/STO films grown at 1 and 0.01 Pa have the same magnetism as La$_{1-x}$Sr$_x$CoO$_3$/STO films when
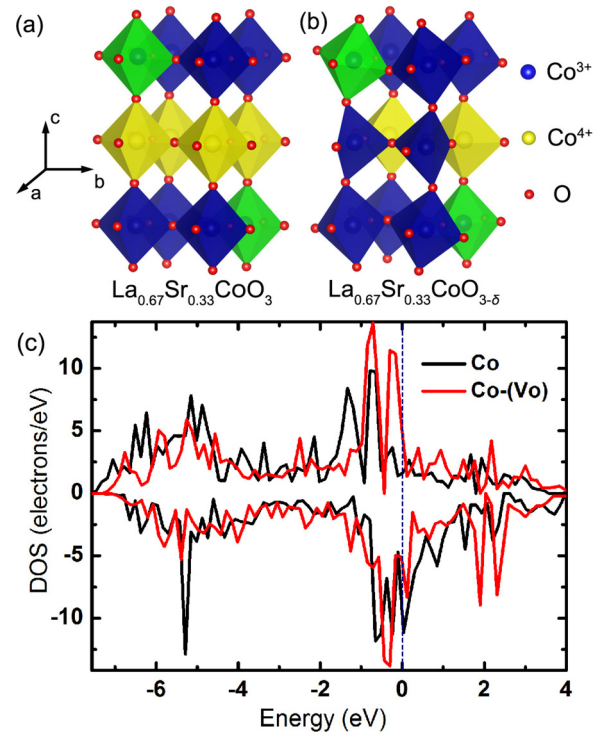

FIG. 6. Calculated models for (a) LSCO and (b) LSCO$_{3-\delta}$. The LS and IS state Co^{3+} cations are marked in blue and green, respectively. The LS state Co^{4+} cation is marked in yellow. (c) Projected DOS for LSCO (black curve) and LSCO$_{3-\delta}$ (red curve). The blue dotted line marks the Fermi energy.

TABLE I. Magnetic moments of oxygen-deficient LSCO films and La$_{1-x}$Sr$_x$CoO$_3$ films [13].

Substrate	Oxygen deficient LSCO films and magnetic moment (μ_B/Co)	Sr-doped LaCoO$_3$ films and magnetic moment (μ_B/Co)
STO	La$^{3+}_{0.67}$Sr$^{2+}_{0.33}$Co$^{3+}_{0.71}$Co$^{4+}_{0.29}$O$^{2-}_{2.98}$, $M_1 = 0.69$	La$_{0.7}$Sr$_{0.3}$CoO$_3$, $M_2 = 0.71$
STO	La$^{3+}_{0.67}$Sr$^{2+}_{0.33}$Co$^{3+}_{0.79}$Co$^{4+}_{0.21}$O$^{2-}_{2.94}$, $M_1 = 0.00$	La$_{0.8}$Sr$_{0.2}$CoO$_3$, $M_2 = 0.00$
LAO	La$^{3+}_{0.67}$Sr$^{2+}_{0.33}$Co$^{3+}_{0.79}$Co$^{4+}_{0.21}$O$^{2-}_{2.94}$, $M_1 = 0.60$	La$_{0.8}$Sr$_{0.2}$CoO$_3$, $M_2 = 0.50$
LAO	La$^{3+}_{0.67}$Sr$^{2+}_{0.33}$Co$^{3+}_{0.96}$Co$^{4+}_{0.04}$O$^{2-}_{2.86}$, $M_1 = 0.12$	La$_{0.95}$Sr$_{0.05}$CoO$_3$, $M_2 = 0.17$

$x = 0.20$ and 0.30, respectively. Interestingly, we get the similar result that the LSCO$_{3-\delta}$/LAO films grown at 1 and 0.01 Pa have the same magnetism with La$_{1-x}$Sr$_x$CoO$_3$/LAO films when $x = 0.20$ and 0.05, respectively. The LSCO$_{3-\delta}$ and La$_{1-x}$Sr$_x$CoO$_3$ films have similar magnetic moments when they have the same Co^{3+}/Co^{4+} ratios. From the above results, we consider that doping Sr into LaCoO$_3$ and removing oxygen from LSCO have a similar effect on magnetism. In other words, for the magnetism of LSCO films, adjusting oxygen pressure during the ablation process has a similar effect as Sr doping. The relationship between the effect of oxygen pressure and Sr doping can be correlated using the equation

$$x = 0.33 - 2\delta, \qquad (2)$$

where x is the Sr-doping content in the La$_{1-x}$Sr$_x$CoO$_3$ films and δ is the content of the oxygen vacancy in the LSCO$_{3-\delta}$ films. This means that both LSCO$_{3-\delta}$ and La$_{1-x}$Sr$_x$CoO$_3$ films have a similar magnetism when they obey Eq. (2).

IV. CONCLUSIONS

LSCO films were prepared at different oxygen pressures during the ablation process. Using XRD and HRTEM, we investigated the chemical expansion and the typical modulated stripes along [001] with oxygen pressure decreased from 50 to 0.01 Pa. Combining the experimental result with the calculated one, we demonstrated that the oxygen vacancy was introduced into the films prepared at low oxygen pressures, and that the introduced oxygen vacancy strongly restrains the spin polarization of Co cations. In addition, for the magnetization of the LSCO film, we found that oxygen pressure has a similar effect as Sr doping. Both La$_{1-x}$Sr$_x$CoO$_3$ and LSCO$_{3-\delta}$ films have similar magnetism when they have the same Co^{3+}/Co^{4+} ratios. A formula was derived to correlate their relation. Our work could shed light on physical insights regarding the relationship between both the chemical and structural nature of LSCO films and their magnetic properties.

[1] S. Medling, Y. Lee, H. Zheng, J. F. Mitchell, J. W. Freeland, B. N. Harmon, and F. Bridges, Phys. Rev. Lett. **109**, 157204 (2012).

[2] V. Krapek, P. Novak, J. Kunes, D. Novoselov, D. M. Korotin, and V. I. Anisimov, Phys. Rev. B **86**, 195104 (2012).

[3] D. Samal and P. S. A. Kumar, J. Phys.: Condens. Matter **23**, 016001 (2011).

[4] J. H. Kwon, W. S. Choi, Y.-K. Kwon, R. Jung, J.-M. Zuo, H. N. Lee, and M. Kim, Chem. Mater. **26**, 2496 (2014).

[5] P. Augustinsky, V. Krapek, and J. Kunes, Phys. Rev. Lett. **110**, 267204 (2013).

[6] H. Hsu, P. Blaha, and R. M. Wentzcovitch, Phys. Rev. B **85**, 140404 (2012).

[7] W. S. Choi, J. H. Kwon, H. Jeen, J. E. Hamann-Borrero, A. Radi, S. Macke, R. Sutarto, F. Z. He, G. A. Sawatzky, V. Hinkov, M. Kim, and H. N. Lee, Nano Lett. **12**, 4966 (2012).

[8] D. V. Karpinsky, I. O. Troyanchuk, L. S. Lobanovsky, A. N. Chobot, C. Ritter, V. Efimov, V. Sikolenko, and A. L. Kholkin, J. Phys.: Condens. Matter **25**, 316004 (2013).

[9] J. Pietosa, A. Wisniewski, R. Puzniak, I. Fita, M. Wojcik, W. Paszkowicz, R. Minikayev, J. Nowak, C. Lathe, S. Kolesnik, and B. Dabrowski, Phys. Rev. B **79**, 214418 (2009).

[10] C. Q. Hu, K. W. Park, A. Posadas, J. L. Jordan-Sweet, A. A. Demkov, and E. T. Yu, J. Appl. Phys. **114**, 183909 (2013).

[11] D. Fuchs, E. Arac, C. Pinta, S. Schuppler, R. Schneider, and H. von Lohneysen, Phys. Rev. B **77**, 014434 (2008).

[12] H. Seo, A. Posadas, and A. A. Demkov, Phys. Rev. B **86**, 014430 (2012).

[13] H. W. Yang, H. R. Zhang, Y. Li, S. F. Wang, X. Shen, Q. Q. Lan, S. Meng, R. C. Yu, B. G. Shen, and J. R. Sun, Sci. Rep. **4**, 6206 (2014).

[14] Z. Németh, A. Szabó, K. Knížek, M. Sikora, R. Chernikov, N. Sas, C. Bogdán, D. L. Nagy, and G. Vankó, Phys. Rev. B **88**, 035125 (2013).

[15] Q. Huang, J. M. Liu, J. Li, H. C. Fang, H. P. Li, and C. K. Ong, Appl. Phys. A **68**, 533 (1999).

[16] Y. W. Li, Z. G. Hu, F. Y. Yue, W. Z. Zhou, P. X. Yang, and J. H. Chu, Appl. Phys. A **95**, 721 (2009).

[17] D. Schumacher, A. Steffen, J. Voigt, J. Schubert, Th. Brückel, H. Ambaye, and V. Lauter, Phys. Rev. B **88**, 144427 (2013).

[18] X. Z. Chen and T. Grande, Chem. Mater. **25**, 927 (2013).

[19] J. Mastin, M. A. Einarsrud, and T. Grande, Chem. Mater. **18**, 6047 (2006).

[20] J. R. Sun, H. W. Yeung, H. Li, K. Zhao, H. N. Chan, and H. K. Wong, J. Appl. Phys. **90**, 2831 (2001).

[21] W. Donner, C. L. Chen, M. Liu, A. J. Jacobson, Y. L. Lee, M. Gadre, and D. Morgan, Chem. Mater. **23**, 984 (2011).

[22] See Supplemental Material at http://link.aps.org/supplemental/10.1103/PhysRevB.93.094421 for density functional theory calculations.

[23] G. Kresse and D. Joubert, Phys. Rev. B **59**, 1758 (1999).